

4 **Abyssal Pathways and the Double Silica Maximum in the Northeast Pacific Basin**

5 **Susan L. Hautala¹ and Douglas E. Hammond²**

6
7 ¹University of Washington.

8 ²University of Southern California.

9
10
11 **Contents of this file**

- 12
13 A. Lagrangian trajectory tracer initialization values (Figure S-A1).
14 B. Additional model fields (Figures S-B1, S-B2).
15 C. Additional model-data comparisons (Figure S-C1).
16 D. Sensitivity experiment (Table S-D1, Figures S-D1, S-D2, S-D3, S-D4).
17

18
19 **Introduction**

20 This supplement contains information about the boundary conditions (supplemental to Figure 1), along with
21 additional model fields and comparisons to observations (supplemental to Figures 1-3).

22 The final section (D) contains a detailed discussion of the sensitivity experiments that were summarized in the
23 text, with additional supporting figures.

24
25
26

A. LAGRANGIAN TRAJECTORY TRACER INITIALIZATION VALUES

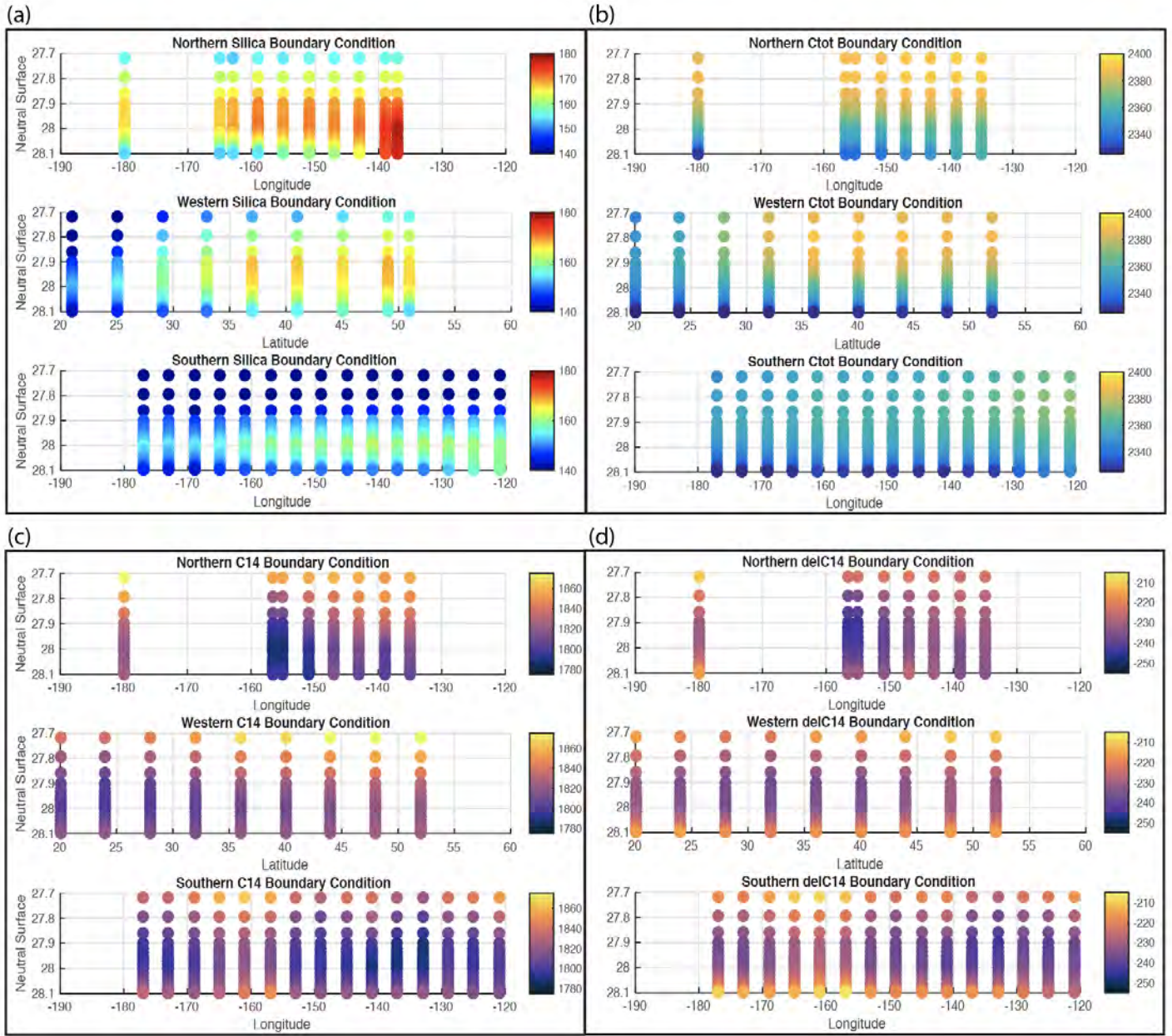


Figure S-A1. Tracer concentration boundary conditions for water parcel trajectories initialized along northern, southern and western lines: (a) Silica ($\mu\text{mol kg}^{-1}$), (b) total Carbon ($\mu\text{mol kg}^{-1}$), (c) ^{14}C Carbon normalized by $^{14}\text{C}/^{12}\text{C}$ ratio in 1950 atmosphere ($\mu\text{mol kg}^{-1}$), (d) $\Delta^{14}\text{C}$ (‰), calculated from (b) and (c).

45

B. ADDITIONAL MODEL FIELDS

The figure displays eight panels of tracer fields, arranged in a 4x2 grid. The top two rows correspond to 42°N, and the bottom two rows correspond to 166°W. The left column shows total carbon (C-Tot) and silica added per age (ΔSi/Δt), while the right column shows carbon-14 anomaly (Δ¹⁴C) and carbon added per age (ΔC/Δt). Each panel is a contour plot with depth on the y-axis (0 to 5000 m) and longitude (180° to 140°W) or latitude (20°N to 50°N) on the x-axis. A black silhouette of the ocean floor is overlaid on each plot. Color bars below each row indicate the values for the tracers.

- Row 1 (42°N):** C-Tot (2350 to 2380 μmol/kg) and Δ¹⁴C (-255 to -205 ‰).
- Row 2 (42°N):** Silica added / Age (0 to 0.2 μmol/kg/yr) and Carbon added / Age (0 to 0.2 μmol/kg/yr).
- Row 3 (166°W):** C-Tot (2350 to 2380 μmol/kg) and Δ¹⁴C (-255 to -205 ‰).
- Row 4 (166°W):** Silica added / Age (0 to 0.2 μmol/kg/yr) and Carbon added / Age (0 to 0.2 μmol/kg/yr).

46

47

48

49

50

51

52

53

Figure S-B1. Additional bin-averaged tracer fields, as labelled. Tracer added is the value for a Lagrangian water parcel found at a given location minus its initial value. Thus, the rates in the lower panels average the time history of Lagrangian parcels found at a given location, and should not be interpreted as a local (Eulerian) flux rate.

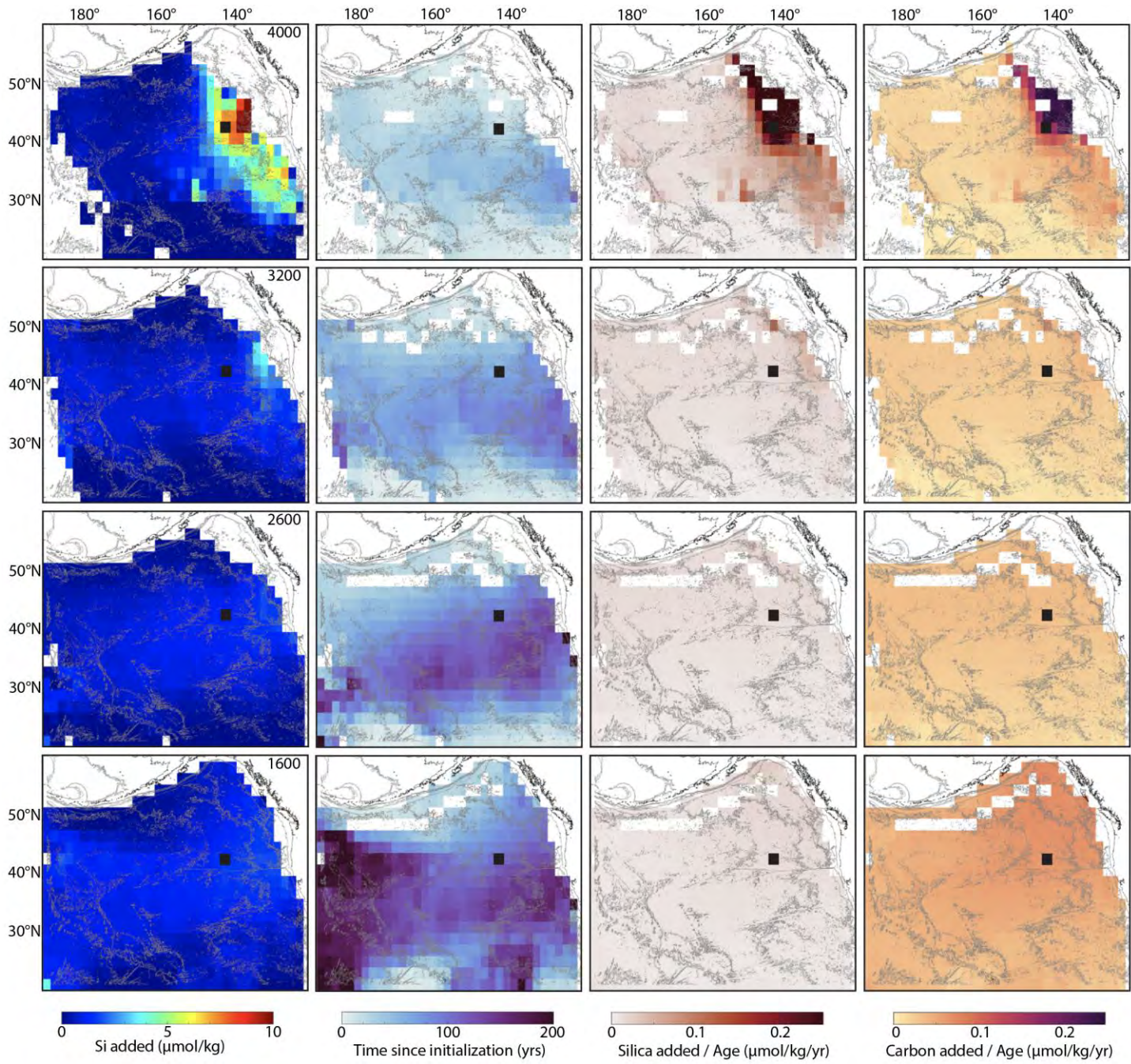


Figure S-B2. Additional bin-averaged variables, on pressure (dbar) surfaces as labelled. The black square marks 42°N, 142°W. Tracer added is the value for a Lagrangian water parcel found at a given location minus its initial value. Thus, the rates in the last two columns average the time history of Lagrangian parcels found at a given location, and should not be interpreted as a local (Eulerian) flux rate.

C. ADDITIONAL MODEL DATA COMPARISONS

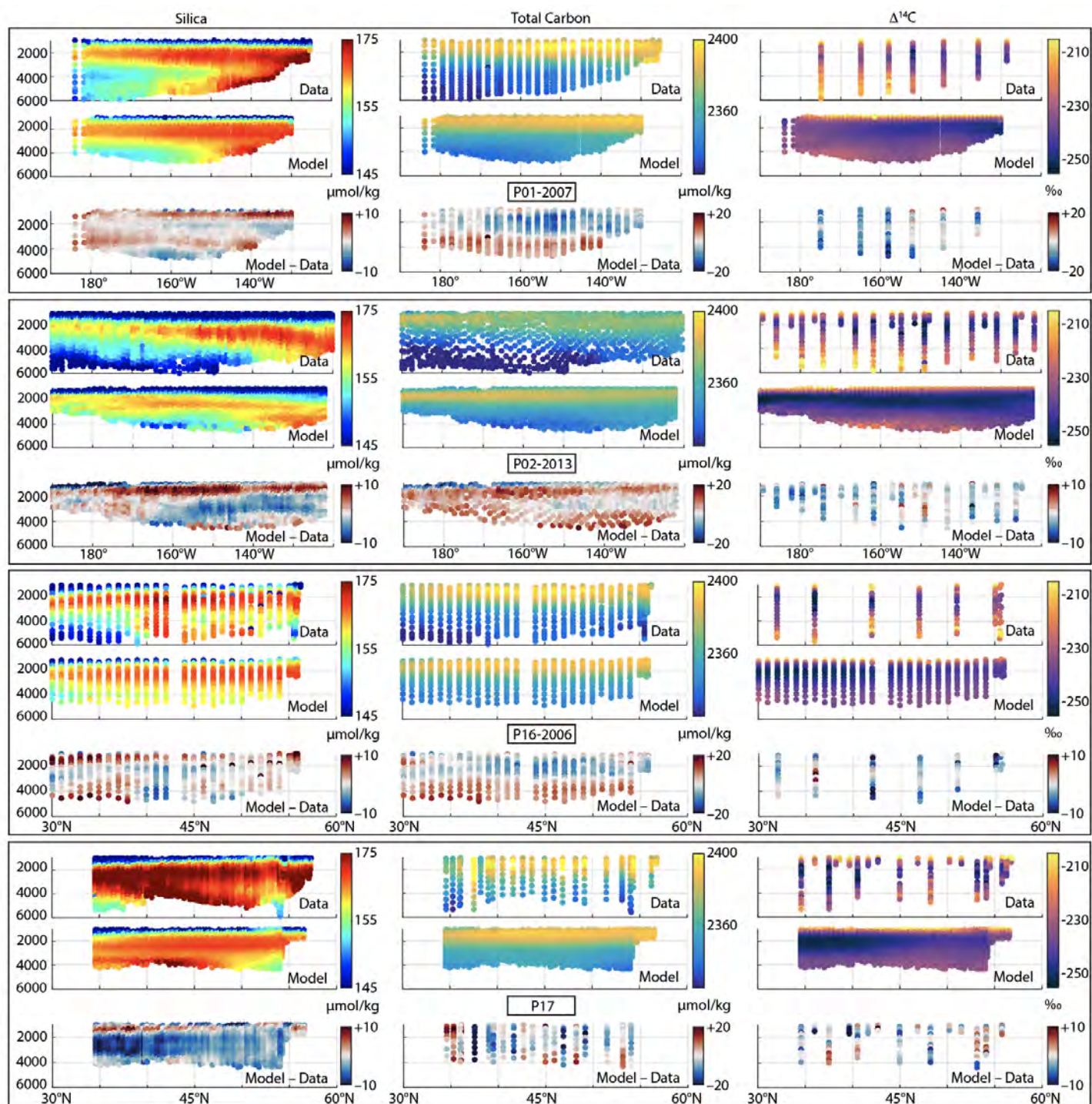


Figure S-C1. Modeled tracer fields interpolated to bottle data locations from hydrographic sections and the model concentration difference from the data. Note that because it is constrained to the UCDW, the model fields do not extend into topographically disconnected deep pools in the north and south NEPB. Top row: P01-2007 along nominal 47°N; 2nd row: P02-2013 along ~30°N; 3rd row: P16-2006 along ~150°W; bottom row: P17 along ~135°W but angling to 160°W in the subarctic gyre.

D. SENSITIVITY EXPERIMENTS

Systematic variations to the assumed parameters were explored via sensitivity experiments using 25 ensemble runs as listed in Table S-D1. It was found that the average radiocarbon bias, relative to the four sections of bottle data examined in this study, was the most sensitive to variations of the lateral diffusivity, K_H , because of this tracer's inherent decay-related clock. In each case, a new inverse model solution (following Hautala 2018) was computed, where the value of lateral diffusivity was specified rather than solved for (Figure S-D3). As K_H is varied, the magnitude of the radiocarbon bias is affected in opposite sense to the magnitude of the silica bias, and also to RMS misfits to the potential vorticity and salinity constraints in the inverse calculation (Figure S-D1), providing a means of manually optimizing the selection of this parameter. A final choice was made by maximizing K_H , considering the estimated 95% confidence limit error for any neutral surface ($\pm 211 \text{ m}^2/\text{s}$) for the solution of Hautala (2018), and its adverse impact on silica bias and inverse model misfit. A 100-ensemble version with the parameters of Run 7 ($K_H = 260 \text{ m}^2/\text{s}$) is interpreted in the main paper. For this solution, the radiocarbon bias is approximately 1% between 1500-3500 m depth, comparable to the error level in deVries et al. (2019). A run that halts trajectories when they dead-end at topographic holes, rather than implementing the “boundary slippage” algorithm (Figure S-D4, compare to Figure 1) loses a great deal of information, especially in the deeper UCDW. However, the double silica maximum still occurs.

Run	σ km	$K_H = 1/2 \sigma^2/\Delta t$ m^2/s	Si_Benthic x [20, 200, 600] $\text{mmol}/\text{m}^2/\text{yr}$	Si_Rain x [1, 10, 90] $\text{mmol}/\text{m}^2/\text{yr}$	CB_Source H value (m)	Si Added (Tmol) 1000-2800	Si Added (Tmol) 2800-5000
1	40	51	[1,1,1]	[1,1,1]	0	55.8	58.3
2	50	81	[1,1,1]	[1,1,1]	0	51.9	62.8
3	60	116	[1,1,1]	[1,1,1]	0	45.9	53.5
4	70	158	[1,1,1]	[1,1,1]	0	39.0	42.4
5	80	206	[1,1,1]	[1,1,1]	0	33.3	41.0
6	85	232	[1,1,1]	[1,1,1]	0	30.9	38.0
7*	90	260	[1,1,1]	[1,1,1]	0	28.3	32.8
8	100	322	[1,1,1]	[1,1,1]	0	24.5	29.5
9	90	260, no KV	[1,1,1]	[1,1,1]	0	27.7	22.6
10	90	260	[1,1,1]	[1,1,1]	10	51.4	37.2
11	90	260	[1,1,1]	[1,1,1]	50	34.4	32.5
12	90	260	[1,1,1]	[1,1,1]	100	31.5	33.3
13	90	260	[1,1,2]	[1,1,0.5]	0	28.3	35.8
14	90	260	[1,2,1]	[1,0.5,1]	0	27.7	33.9
15	90	260	[1,2,2]	[1,0.5,0.5]	0	28.7	36.2
16	90	260	[1.05,1.05,1.15]	[0,0,0]	0	27.5	23.1
17	90	260	[1,1,1]	[1,1,0.33]	0	27.5	20.9

Table S-D1. Sensitivity study parameters using 25 ensemble runs. The total addition of silica in NPDW and UCDW layers during one pass of the water parcels through the basin is reported in the final two columns. Note that for Run 7, a 100 ensemble run is discussed in the text, leading to minor differences in these values.

Random Gaussian displacement:

Runs 1-8 explored the effects of varying the value of the lateral (along neutral surface) displacement after each time step (equivalently, K_H). Larger values of lateral diffusivity increase the misfit in the potential vorticity and salinity conservations equations that are the basis of this circulation inverse (Figure S-D1 top left). As a final experiment (Run 9), the diapycnal displacement (corresponding to K_V) is set to zero, with only minor impact on bias.

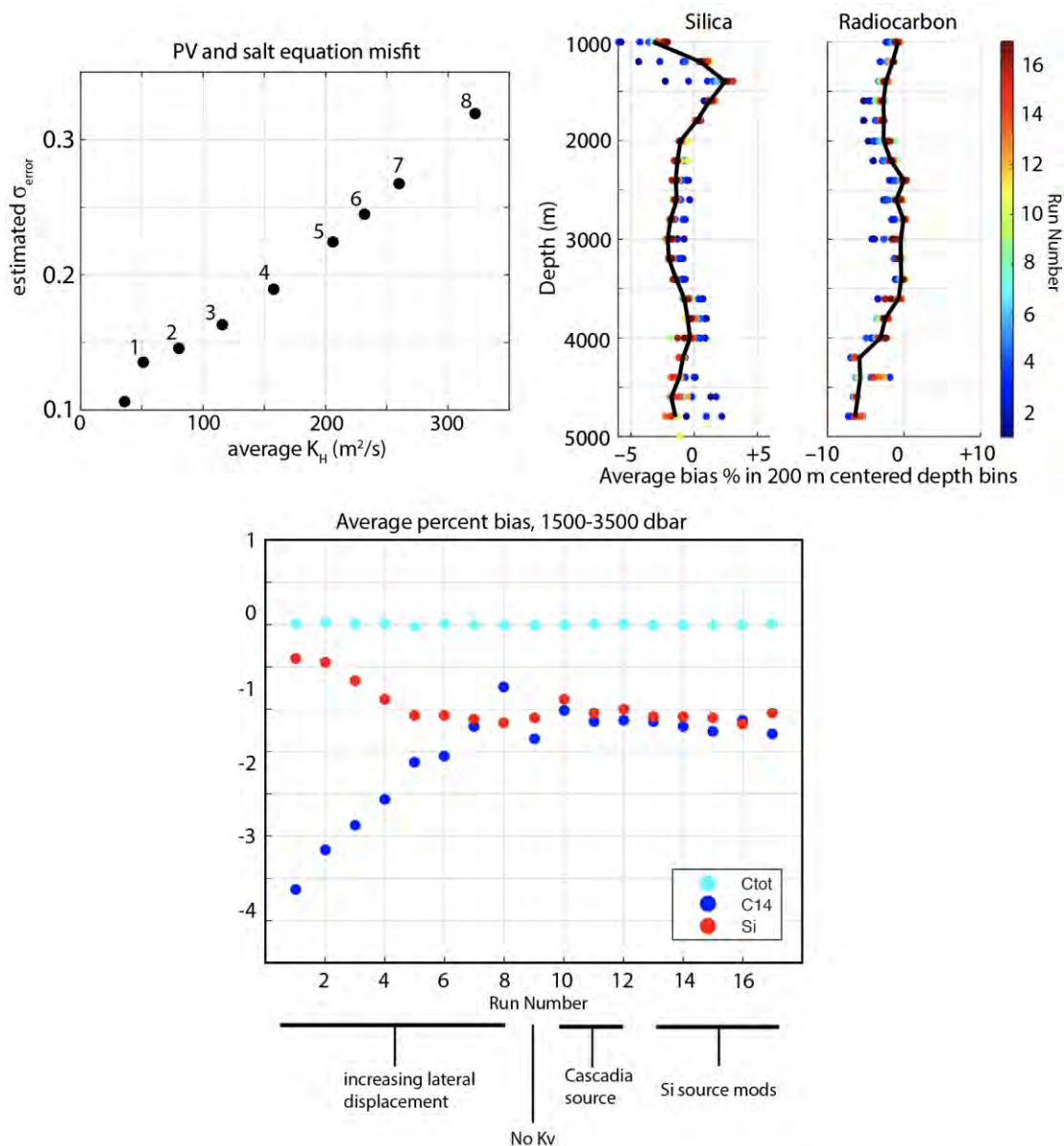
Cascadia Basin source:

Runs 10-12 explored the addition of a Cascadia Basin source. If, after a given time-step, a trajectory point was located east of 132°W , between 44°N and 48°N and between 2100 to 2700 dbar, the silica flux was augmented by $0.81 \text{ mmol}/\text{m}^2/\text{yr}$ (Esther et al. 2010), divided by a (boundary layer) height indicated in the right-most column of Table S-D1, converted to $\mu\text{mol}/\text{kg}/\text{yr}$. Adding the most extreme version of the Cascadia Basin source

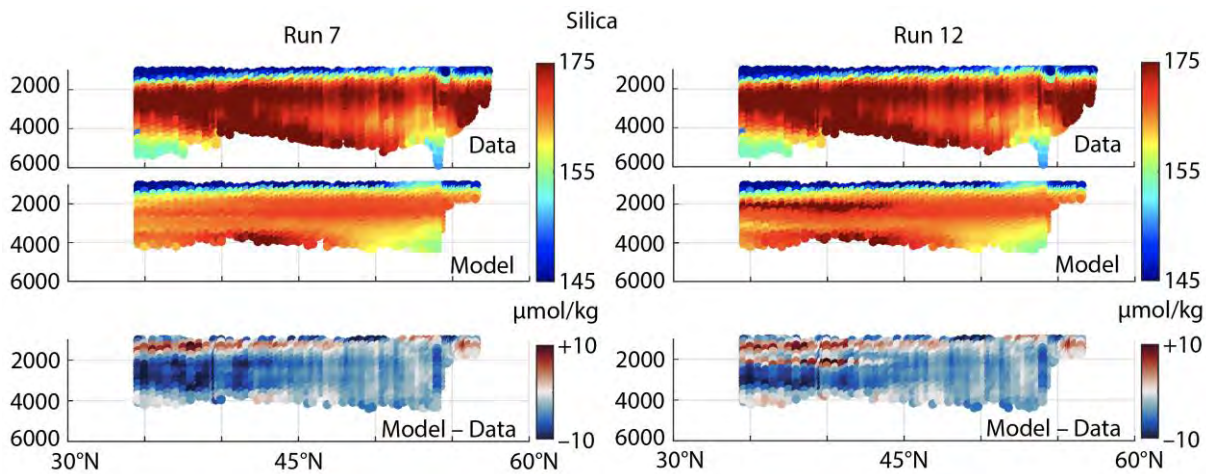
118 (dividing the total flux by the smallest vertical layer thickness (10 m) had little effect on the basin wide average
 119 bias, but it did improve agreement along P17 for the mid-depth maximum (Figure S-D2).
 120

121 *Silica source function:*

122 Runs 13-17 explored modifications of aspects of the silica source function. While the total amount of silica
 123 (right columns of Table S-D1) is impacted, there is little change in basin-average bias (Figure S-D1). Because
 124 silica tends to be biased low below 2000 m and biased high above that level, we explored increasing the bottom
 125 source in the transitional and subarctic bands separately and then together while halving the water column
 126 source. Next (Run 16), we set the water column source to zero and increased the bottom source proportionally.
 127 Finally (Run 17), we set the subarctic water column source to 5% of the bottom source (the same percentage as
 128 the other latitude bands).
 129

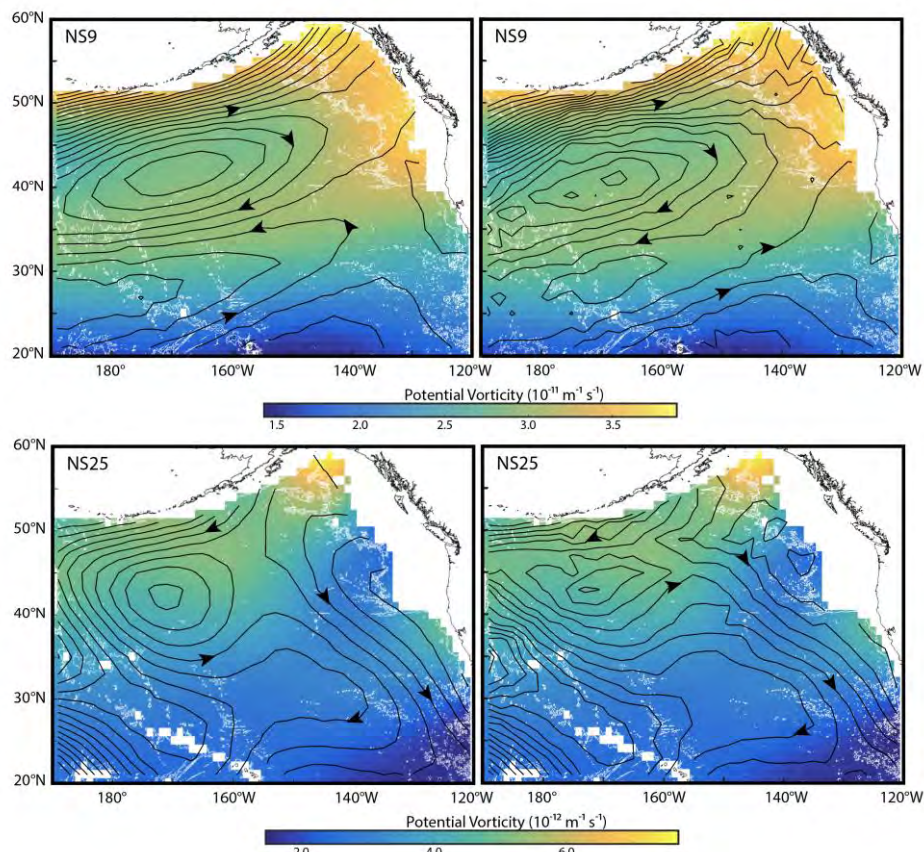


130
 131
 132 *Figure S-D1. Top left:* RMS error standard deviation from the inverse fit to potential vorticity and salt equations
 133 using specified values of lateral diffusivity. The left-most data point corresponds to the solution in Hautala
 134 (2018) which has a depth-averaged $K_H = 36 \text{ m}^2/\text{s}$. Values for sensitivity run numbers (Table S-D1) are indicated
 135 next to the points. *Top right:* Average percent bias for silica and radiocarbon as a function of depth (compared
 136 to the four repeat hydrography sections discussed in the main text) colored by run number. *Bottom:* Average
 137 percent bias for 1500-3500 m as a function of run number for each of the three simulated tracers.



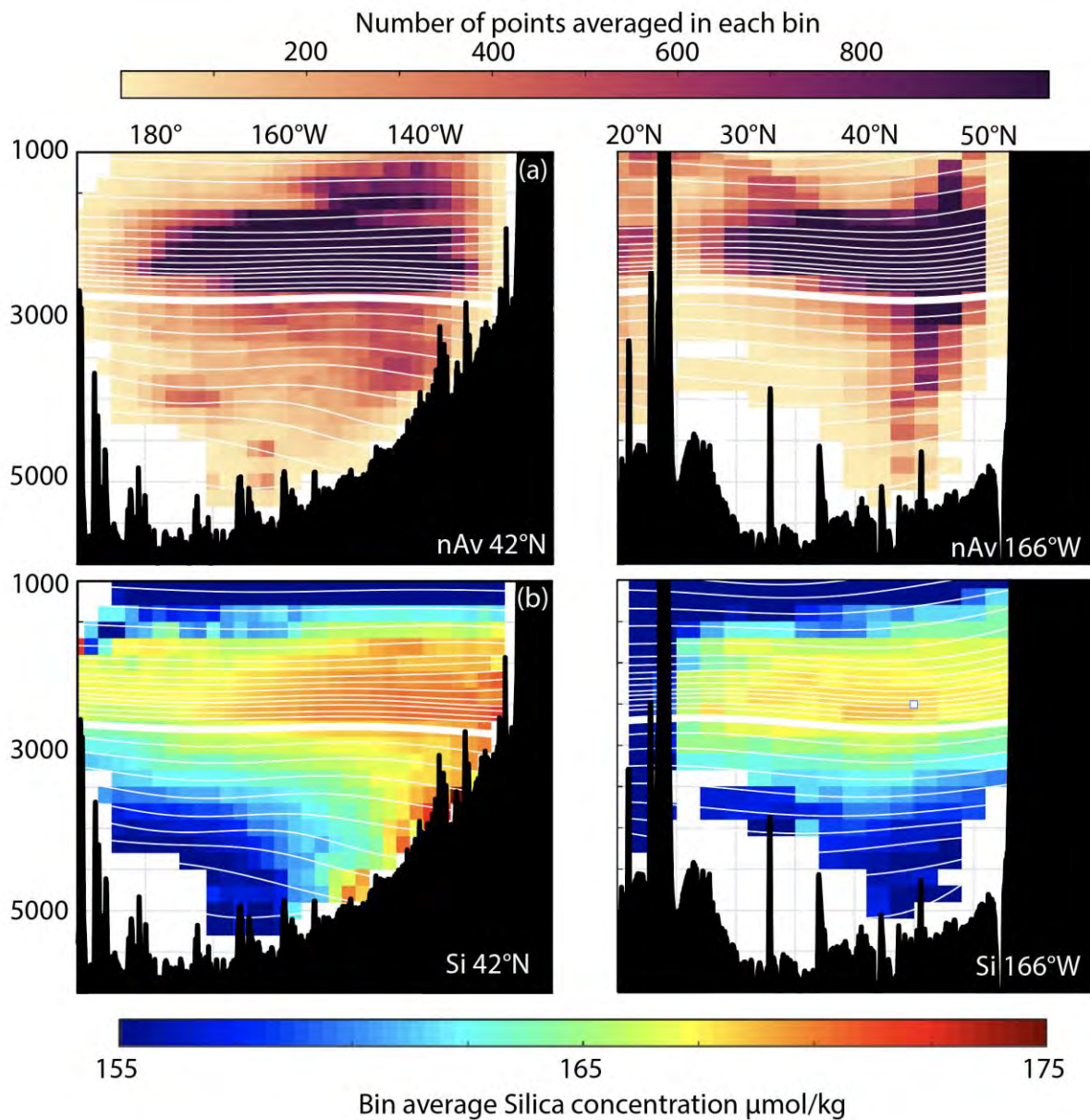
139
140
141
142
143
144
145

Figure S-D2. Model-data comparison along P17 without (Run 7) and with (Run 12) a crude Cascadia Basin silica source. Of the three experiments with this additional source, Run 12 distributes the estimated seafloor source from Esther et al. (2010) over the smallest depth range (10 m, see Table S-D1) and thus has the greatest impact on concentration.



146
147
148
149
150
151
152
153
154

Figure S-D3. Left: flow fields and potential vorticity from the inverse model where the lateral diffusivity is solved for as a least-squares fit to potential vorticity and salinity conservation equations (Hautala 2018). Right: flow and potential vorticity from an inverse solution where lateral diffusivity is specified at $K_H = 260 \text{ m}^2/\text{s}$ (Run 7 value). Potential vorticity is colored and absolute geostrophic streamfunction is contoured (by $0.02 \text{ m}^2/\text{s}^2$) in black with flow directions indicated. Top: $\gamma = 27.795 \text{ kg m}^{-3}$, lying in the middle of the NPDW. Bottom: $\gamma = 27.795 \text{ kg m}^{-3}$, lying in the middle of the UCDW. Increased misfit in the potential vorticity and salinity equations with increasing lateral diffusivity manifests as noise in the right panel streamfunction contours.



155
 156
 157
 158
 159
 160
 161
 162
 163
 164
 165
 166
 167
 168

Figure S-D4. Vertical sections (see Figure 1 for comparison) for a 100-ensemble run where the boundary slippage algorithm is turned off. While the number of points to average for each Eulerian bin decreases, particularly in the UCDW, the double silica maximum still emerges.